Electrochimica Acta 55 (2010) 1272–1277

Contents lists available at ScienceDirect

Electrochimica Acta

journal homepage: www.elsevier.com/locate/electacta

Diffusion-limited chronoamperometry at conical-tip microelectrodes

Dieter Britz[a,*,1], Shaneel Chandra[b], Jörg Strutwolf[c], Danny K.Y. Wong[b]

[a] Department of Chemistry, Aarhus University, 8000 Århus C, Denmark
[b] Department of Chemistry and Biomolecular Sciences, Macquarie University, Sydney, NSW 2109, Australia
[c] Tyndall National Institute, Lee Maltings, Cork, Ireland

ARTICLE INFO

Article history:
Received 31 August 2009
Received in revised form 8 October 2009
Accepted 8 October 2009
Available online 10 November 2009

Computational electrochemistry
Digital simulation
Conical-tip microelectrodes

ABSTRACT

In this paper, we present simulated diffusion-limited time-variant currents at conical-tip microelectrodes fabricated by depositing a carbon film in and on pulled quartz capillaries. These mechanically strong microelectrodes are suitable probes for detecting neurotransmitters *in vivo*. The simulated results show that the currents obtained at conical-tip microelectrodes are larger than those at finite conical microelectrodes (e.g. etched carbon fibres protruding from an insulating plane) of comparable dimensions. The currents at conical-tip microelectrodes and finite conical microelectrodes both converge to that of a microdisk electrode at small cone heights and large cone angles, and to that of a cylindrical electrode portion of equal length and half the radius at large cone heights and small cone angles. At short times (scaled by the electrode dimensions), Cottrellian current is achieved at conical-tip microelectrodes and the current densities collapse to the expected chronoamperometric response at a microdisk electrode, subject to some simulation errors. Comparison between a simulated chronoamperogram and an experimental chronoamperogram then allows an estimate of parameters (such as electrode surface area and dimensions) that define the electrode geometry. Steady-state currents based on empirical functions have also been computed for conical-tip microelectrodes and finite conical microelectrodes.

1. Introduction

Coupled with anatomical, physiological and pharmacological evidence, tremendous advances have been made in applying electrochemical techniques to the rapid, real-time *in vivo* analysis of neurotransmitters in specific brain regions [1–5]. This partly arises from the ease of oxidation of several neurotransmitters (dopamine, noradrenaline, serotonin, etc.) at an electrode surface. Another contributing factor stems from significant developments of physically small electrodes that are suitable for implantation into living tissues with minimal physical damage. For example, by recording cyclic voltammograms of dopamine at carbon fibre microelectrodes implanted in the brain of freely moving rats, Hermans et al. demonstrated that cocaine causes significant fluctuations in dopamine concentration in the brain [1]. Following the electrophoretic separations of cytoplasmic samples, Woods et al. relied on the amperometric detection of dopamine at a 2.5 μm diameter carbon fibre electrode to estimate an average cytoplasmic dopamine concentration of 240 μM in rat pheochromocytoma cells [2].

Our laboratory [6] has previously reported the fabrication of physically small carbon electrodes by pyrolysing acetylene gas on quartz capillaries that had been pulled down to a typical 2–5 μm tip diameter. Compared to carbon fibre electrodes of a similar dimension, physically small carbon electrodes were found to show an improved signal-to-noise ratio in detecting dopamine *in vivo* [7]. More recently, after hydrogenating these carbon electrodes, they showed similar effectiveness against electrode fouling to diamond electrodes in detecting dopamine [8].

In this paper, we will focus on a study of the response of physically small carbon electrodes to a potential pulse and the resulting steady-state current. As presented below, fitting simulated chronoamperometric signals to those obtained at physically small carbon electrodes has enabled better estimates of such parameters as the radius and the axial length to define them as electrodes with a conical tip. Therefore, we will hereafter refer to them as conical-tip microelectrodes (CTME). As shown in Fig. 1A, a CTME is characterised by the radius a of the carbon deposit at the electrode base, and the base-to-tip length h measured along the axis of the cone. This yields an angle α, which denotes the inclination of the wall to the axis of the cone. This inclination angle is given by

$$\alpha = \tan^{-1}\left(\frac{a}{h}\right). \quad (1)$$

* Corresponding author. Tel.: +45 89423874; fax: +45 86196199.
E-mail addresses: britz@chem.au.dk (D. Britz), schandra@cbms.mq.edu.au (S. Chandra), jorg.strutwolf@tyndall.ie (J. Strutwolf), danny.wong@mq.edu.au (D.K.Y. Wong).
[1] ISE member.

0013-4686/$ – see front matter © 2009 Elsevier Ltd. All rights reserved.
doi:10.1016/j.electacta.2009.10.025

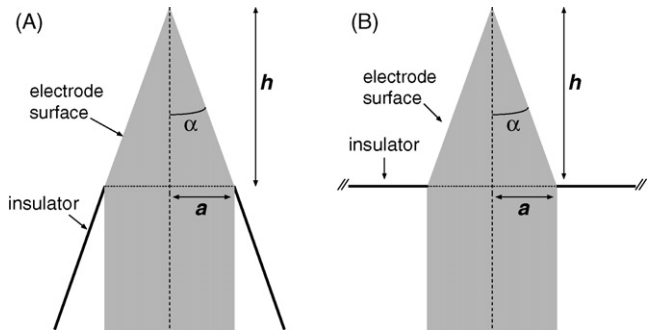

Fig. 1. Schematic of the present conical-tip electrode (CTME) (A) and the similar electrode of Zoski and Mirkin's finite conical electrode (B).

These electrodes are modelled based on an idealised geometry consisting of sharp cones with negligible disk area at the tip. This is an acceptable assumption as the disks are small in comparison to the length of the carbon film along the cone walls.

Previously, Zoski and Mirkin reported a simulation study of finite conical microelectrodes fabricated by sealing an etched carbon fibre in an insulator such that a defined length of the fibre protrudes from the insulating plane [9], as depicted in Fig. 1B. We have defined α in Fig. 1B in a manner that is consistent with that shown in Fig. 1A, whereas in [9], the angle was defined as that of the wall to the base. Dickinson et al. have presented some additional simulation results of these finite conical electrodes, extending the study to include simulation of linear and cyclic voltammetry [10]. Notably, the insulating plane at a finite conical microelectrode limits mass transport to the base edge of the electrode, whereas the base edge on a CTME is more accessible. Both types of conical electrodes become identical to an ultramicrodisk electrode (UMDE) when $h \to 0$, and this is a useful verification of the simulations shown later in this paper. At the other extreme, CTME with a large h/a ratio (i.e. a very sharp cone) will have a response similar to that of a cylindrical electrode of radius $0.5a$ and length h, ignoring edge effects. Overall, the circular disk and cylinder represent extreme cases of a very low ($h/a \to 0$) and a very tall cone ($h/a \to \infty$), respectively. As will be seen below, the CTME deviates significantly in its chronoamperometric response from the finite conical electrode.

The present work aims to present simulation results, both time-dependent and steady state, for the current at a CTME under diffusion limiting conditions. We will then compare these results to those of finite conical microelectrodes. In addition, simulated results will also be compared to experimental results for the reduction of $Ru(NH_3)_6^{3+}$ at CTMEs.

2. Theory

The diffusion equation for our system is

$$\frac{\partial c}{\partial t} = D\left(\frac{\partial^2 c}{\partial z^2} + \frac{1}{r}\frac{\partial c}{\partial r} + \frac{\partial^2 c}{\partial r^2}\right) \tag{2}$$

in which c is concentration, t the time, D the diffusion coefficient, z the vertical axis in the direction of the central axis of the cone and r is the radial coordinate. We define a maximum distance L from points on the electrode, over which there are significant changes in concentration during a given time, given by [11],

$$L = 6\sqrt{T} \tag{3}$$

(T is defined in (4d)), so that L depends on the largest value of T to which the simulation is driven. The quantity L will be used in constructing a suitable spatial grid for the simulation, as further explained below.

It is convenient to normalise (2) using the following dimensionless symbols:

$$C = \frac{c}{c^*} \tag{4a}$$

$$Z = \frac{z}{a} \tag{4b}$$

$$R = \frac{r}{a} \tag{4c}$$

$$T = \frac{Dt}{a^2} \tag{4d}$$

$$H = \frac{h}{a}, \tag{4e}$$

where c^* is the initial bulk concentration of the electroactive species. With these normalisations, the electrode has unity radius R at its base and a height H. Then, (2) becomes

$$\frac{\partial C}{\partial T} = \frac{\partial^2 C}{\partial Z^2} + \frac{1}{R}\frac{\partial C}{\partial R} + \frac{\partial^2 C}{\partial R^2}. \tag{5}$$

2.1. Cylinder approximation

In what follows, the term "cylinder" refers to a portion of a given length of an infinitely long cylinder, for which there is some theory. As mentioned above, there are approximate solutions for the extreme cases. For very small α, where the cone approximates a cylinder of length h and radius $0.5a$, Szabo et al. [12] provide a solution for the current holding within 1.3% for all times,

$$i_{cyl} = 2\pi nFDc^* hf(\theta) \tag{6}$$

with

$$f(\theta) = \frac{\exp(-0.1\sqrt{\pi\theta})}{\sqrt{\pi\theta}} + \frac{1}{\ln(\sqrt{4\exp(-\gamma\theta)} + \exp(5/3))} \tag{7}$$

in which γ is Euler's constant (0.5772156...), n is the number of electrons transferred, F is the Faraday constant, D the diffusion coefficient and c^* the bulk concentration of the electroactive substance, and θ is the normalised time defined by $\theta = Dt/a^2$, where a is the radius of the cylinder. This is equivalent to definition (4d), but a different symbol is used to highlight the fact that the cone and cylinder have different radii when being compared (see below). The factor 2 in (6) is based on the assumption of a whole cylinder, rather than a hemicylinder, as was the case in Szabo et al. As shown below, for a CTME with large H, this equation fits the simulated currents rather well. At short times, Szabo et al. have

$$f(\theta) = 0.5 + \frac{1}{\sqrt{\pi\theta}}. \tag{8}$$

The actual current in amperes for this case is

$$i = 2\pi nFDc_b h\left(\frac{1}{2} + \frac{a}{\sqrt{\pi Dt}}\right). \tag{9}$$

Hence, based on a linear plot of current against $t^{-1/2}$, the y-intercept will provide an estimate of h, and the slope will yield the radius a of a CTME in the solution of an electroactive species of known concentration.

Note that if a cone current is to be compared to that at a cylinder, then the above equations must be evaluated setting the radius to half that of the cone base. This results in the relation $\theta = 4T$.

2.2. Disk approximation

For a disk electrode, we have the approximation formulae by Mahon and Oldham [13] which, using our present normalisations

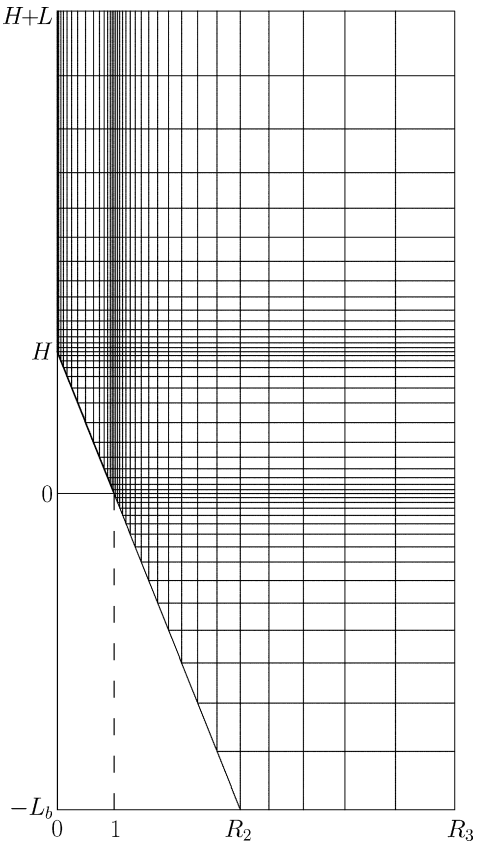

Fig. 2. Example simulation grid.

are, for $T \leq 0.53$,

$$I = \frac{\pi}{4}\left((\pi T)^{-1/2} + 1 + \frac{1}{2}\left(\frac{T}{\pi}\right)^{1/2} - 0.12003\,T + 0.013273\,T^{3/2}\right) \tag{10}$$

and for $T > 0.53$

$$I = 1 + \frac{\pi}{4}(8\pi^{-5/2}\,T^{-1/2} + 8.9542 \times 10^{-3}\,T^{-3/2} - 2.5664 \times 10^{-4}\,T^{-5/2} - 2.2312 \times 10^{-4}\,T^{-7/2} + 2.7628 \times 10^{-5}\,T^{-9/2}). \tag{11}$$

This pair of equations was found [14] to be accurate to approximately 0.03% over the whole T range, using the branching point in T as above, sufficient for present purposes. The current in actual dimensions can be obtained by multiplying by the Saito steady-state value for a disk electrode [15],

$$i = 4nFc^*Da. \tag{12}$$

As with the cylinder, there is a limiting form at small T,

$$I = \frac{\pi}{4}\left(1 + \frac{1}{\sqrt{\pi T}}\right) \tag{13}$$

which has the same slope as the equivalent form for the cylinder.

2.3. The simulation

A grid as shown in Fig. 2 (coarsely spaced for visibility) was generated in the form of a series of points along R and another of points along Z. This is an adaptation of the grids used previously for other geometries [16,17] to the present electrode. As in those works, grid generation was found to be the major problem in the simulation. To satisfy the spatial extent L, apart from points along that part of the cone wall covered by the carbon film, the grid must include an extra height L above the cone tip and a length L down along the insulating cone wall below the carbon base, meeting the grid floor at $R = R_2$ and $Z = -L_b = L\cos\alpha$, Z being defined as zero at the electrode base. The left hand boundary of the grid is the axis of the cone, and the right-hand boundary at $R = R_3 = 1 + L$. The insulating part of the cone wall is thus marked as the region $1 < R \leq R_2$, shown in Fig. 2. Along this distance and along the electrode, we have $Z = (1 - R)H$. These specifications are needed for the boundary conditions, which are

$$\begin{aligned}
T < 0, \quad \text{all } R, Z \quad &: \quad C = 1 \\
T > 0 \quad &: \\
0 \leq R \leq 1, \quad Z = (1-R)H \quad &: \quad C = 0 \\
1 < R \leq R_2, \quad Z = (1-R)H \quad &: \quad \frac{\partial C}{\partial w} = 0 \\
Z = -L_b, \quad R_2 < R < R_3 \quad &: \quad \frac{\partial C}{\partial Z} = 0 \\
R = 0, Z > H \quad &: \quad \frac{\partial C}{\partial R} = 0 \\
R \geq R_3, \quad \text{all } Z \quad &: \quad C = 1 \\
Z \geq H + L, \quad \text{all } R \quad &: \quad C = 1.
\end{aligned} \tag{14}$$

Here, w is the direction normal to the cone wall.

After normalising the current I by the Saito steady-state value at a UMDE (12)[15], we obtain

$$I = \frac{\pi}{2\cos\alpha}\int_0^1 R\frac{\partial C}{\partial w}\,\mathrm{d}R. \tag{15}$$

The derivative $\partial C/\partial w$ is given by

$$\frac{\partial C}{\partial w} = \frac{\partial C}{\partial Z}\sin\alpha + \frac{\partial C}{\partial R}\cos\alpha. \tag{16}$$

Computed currents are compared with those at the disk electrode as seen above in (10) and (11), and with currents at a cylinder, setting the cylinder radius at 0.5 and the length equal to H. As discussed below, these two models produce results very close to simulated CTME currents at, respectively, very low and high H.

3. Computational

Owing to a lack of analytical solutions, separate computations using two completely different methods, the commercial program COMSOL which uses finite elements, and a simulation program written in Intel Fortran 95, both implementing the above theory, were used to ensure the validity of the results. Both were carried out on a PC running under Linux and IEEE 754 standard double precision, giving approximately 16-decimal precision.

For the Fortran program, the integration in (15) was done using three-point gradient approximations in both the Z and R directions and the trapezium integration rule. The grid, a coarsely divided example of which is illustrated in Fig. 2, was generated so that there was an exponential expansion of the grid point intervals starting with a minimum distance of normally 0.0001 at both the electrode tip and base, expanding away from these points. Exponentially expanding intervals were first suggested by Seeber and Stefani [18] and Feldberg [19]. The main parameter in the Fortran simulation was N, the number of points for the radial and Z-lines along the electrode wall. The same number of Z-lines was generated above the cone tip, and down along the insulating wall. Along the grid floor, R lines generated along the insulating wall were allowed

to continue expanding to the right of R_2 until a point was reached where R exceeded R_3, which became the right-hand limit where bulk concentration was assumed. The top of the grid always lies at $Z = H + L$. An additional single line of points was placed above this line, and to the right of the farthest right-hand R, because discretisation was expressed using four-point approximations, to achieve discretisation errors of $O(\delta X^2)$, where δX is the interval size in R or Z [11,20]. These outlying points were placed so that there were three equally spaced points at the top and right-hand side of the grid.

The problem of the $1/R$ term in (5) on the cone axis above the cone tip was circumvented in the manner detailed by Britz [11] (page 217) and described previously by Gavaghan [16] and Crank and Furzeland [21]. It uses the McLaurin expansion, reducing the equation to one without the offending term. Then symmetry was assumed at the axis, by setting a fictitious point to the left of the axis, with concentration values equal to those immediately to the right of the axis and using a simple three-point approximation for the derivatives there.

Coefficients for the four-point approximations were computed using the Fornberg algorithm [22]. The temporal first derivative, the left-hand side of (5), was discretised as the three-point backward differentiation formula (BDF) [23,24], introduced in electrochemistry by Mocak and Feldberg [25]. The startup problem [26] was eliminated by starting each simulation with a single backwards implicit step [27]. Three-point BDF has discretisation errors of $O(\delta T^2)$, matching the order of the spatial approximations. The generated grid, as described above, contained approximately $3N \times 2N$ points, and thus that number of unknowns to be solved for, and computations were limited by memory constraints to $N = 90$, leading to a sparse system of about 300,000 entries, hence the limit. This was sufficient however, and results matched those from the COMSOL simulations to approximately 3 decimals. The grid points were numbered and the discretised equations for all points cast into a large sparse system, which was solved by the suite of routines `MA28`[28], available at the Harwell site [29]. `MA28` is a sparse solver allowing LU decomposition [30], which was useful here, since the system consisted of constant coefficients for a given H. A typical simulation required a few minutes of computing time.

Simulations were also performed using the commercial finite element program package COMSOL Multiphysics (version 3.5, COMSOL Ltd., Hertfordshire, UK). Meshes were generated from triangular elements. At the points of the electrode edges and along the line of the electrode surface, free mesh parameters were used with a maximal element size between 0.00001 and 0.002 and an element growth rate of 1.1. The mesh refinement resulted in 20,000 to 100,000 elements. In the software package, the built-in direct sparse matrix solver UMFPACK [31] was used to solve the system of equations. Both approaches led to the same results within the number of decimals presented here, confirming the validity of the programs.

Both COMSOL model reports and Fortran programs can be obtained on application to the authors, respectively JS and DB.

Steady-state currents were also simulated for both the CTME and the finite conical electrode. This was solved after setting the left-hand side of (5) to zero. For these, a problem was to determine the diffusion space limits (the observation time is infinite). This was done by experimenting with some L, and it was found that setting L to about 600 was sufficient. A larger L value did not significantly change the steady-state current. For the finite conical electrode, the radius of the insulating plane was also set at L, effectively infinite. A set of steady-state currents for both electrodes were then approximated by a curve of the form $I = 1 + pH^q$, as was done by Zoski and Mirkin [9] and the parameters determined by using the "fit" procedure built into gnuplot [32]; the procedure is based on a nonlinear least-square Marquardt–Levenberg algorithm.

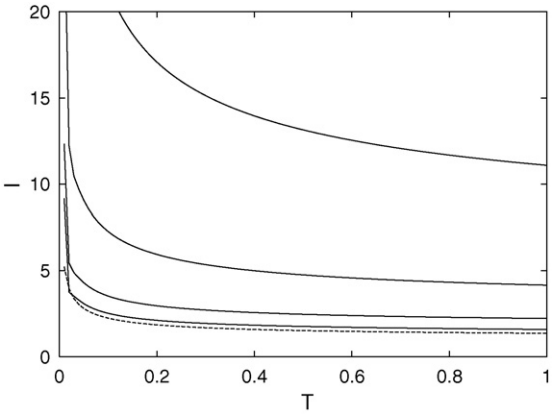

Fig. 3. Current curves. Top to bottom: $H = 30$, 10, 3, 1 and UMDE, respectively.

4. Experimental

CTMEs were fabricated using a previously reported procedure [6]. Briefly, quartz capillaries were initially pulled down to a fine tip. Each capillary was then housed in a larger quartz capillary. Acetylene gas flowing through the pulled capillary was then thermally pyrolysed in the presence of a counter stream of nitrogen gas flowing through the larger capillary. This process resulted in a carbon deposit both at the tip of the pulled capillary and on its shank. Graphite powder and a conducting wire were introduced through the larger end of the pulled capillary to accomplish electrical connection with the carbon deposit. All electrodes were initially tested by cyclic voltammetry of 1.0 mM $Ru(NH_3)_6^{3+}$ (purchased from Strem Chemical Inc., MA, USA) in 0.1 M KCl (Univar) as supporting electrolyte. The solution was degassed with nitrogen for 5 min prior to voltammetric experiments. All electrochemical measurements were carried out using a potentiostat capable of measuring down to picoampere levels (eDAQ Pty Ltd., Sydney, Australia). The potentiostat was operated using version 2.0.14 Echem software on a PC via a 2-channel E-corder interface (eDAQ Pty Ltd.) with 16-bit a/d conversion. A conventional three-electrode cell consisting of a Ag/AgCl reference electrode, a Pt coil auxiliary electrode and a CTME working electrode was used. All measurements were carried out in an aluminium Faraday cage to isolate interferences from the mains and other sources. Chronoamperometry of $Ru(NH_3)_6^{3+}$ at a CTME was performed by applying a resting potential of 300 mV for 2 s, followed by a cathodic potential pulse of −350 mV for 20 s.

5. Results and discussion

Fig. 3 shows simulated chronoamperometric CTME currents for stated H values and, the lowest curve, the current at a microdisk. It is seen that for small H, CTME currents are close to those at a disk, and become larger as H increases. For large H, the current is closer to that at a cylinder of length H and radius 0.5. There is some inherent inaccuracy at small T (that is, after just a few simulation steps), giving rise to an apparent corner in the curve for $H = 1$, which appears to dip below that for the disk electrode at that point. Table 1 shows the ratios of CTME and finite cone electrode currents to currents at a UMDE and cylinder for some H, and the table shows the effect clearly, for both electrodes. Therefore, for a sharply pointed CTME or finite conical electrode ($H \geq 20$), the equation of Szabo et al. [12] adequately describes the CTME current within a few percent.

Steady-state currents for selected H are tabulated in Table 2. Here, currents at the CTME are larger than those at the finite conical electrode, because at the latter, the insulating base that the electrode protrudes from limits the current to some extent. The values we obtained for the finite conical electrode are somewhat smaller

Table 1
Relation of currents I to to those at an UMDE (I_{UMDE}) and cylinder currents (I_{cyl}) at $T = 1$ and various H.

H	Present study		Zoski et al.	
	I/I_{UMDE}	I/I_{cyl}	I/I_{UMDE}	I/I_{cyl}
0.03	1.01	44	1.00	43
0.10	1.05	14	1.02	13
0.30	1.2	5.0	1.08	4.7
1.00	1.6	2.1	1.38	1.8
3.00	3.0	1.3	2.6	1.11
10.00	8.1	1.05	7.5	0.98
30.00	23	0.98	22	0.96

Table 2
Steady-state currents at the CTME and Zoski and Mirkin's finite conical electrode.

H	CTME	Finite conical electrode
0.03	1.014	1.002
0.10	1.058	1.017
0.30	1.186	1.066
1.00	1.656	1.289
3.00	2.745	2.029
10.00	5.621	4.360
20.00	9.010	7.262
30.00	12.08	9.940

at larger H than reported by Zoski and Mirkin. Dickinson et al. [10] also obtained slightly smaller values. The difference between our values and those reported by Zoski and Mirkin is however only a few percent. The function of steady-state current against H is not linear on a log–log scale, so that a simple power function will not fit very well. However, reasonable fits within some percent can be obtained. Simulations for H values up to 30 were fitted and for the CTME this was found to be

$$I = 1 + 0.7156H^{0.8062} \tag{17}$$

which produces a curve matching the simulated values with a maximum error of approximately 7% at small H, decreasing to less than 1% for $H > 6$. For the finite conical electrode, the fit was

$$I = 1 + 0.4058H^{0.9112} \tag{18}$$

which deviates somewhat from Zoski and Mirkin's fit, and the maximum error is 9%. Zoski and Mirkin only fitted to simulated values up to $H = 3$. If we restrict ours to $H = 4$, then the fitted curve becomes

$$I = 1 + 0.2976H^{1.114}, \tag{19}$$

much closer to their parameters (0.3066, 1.144), and the maximum error is now 1.1%. In practice, use of these formulae will depend on the H values used. It is possible that the electrodes of Zoski and Mirkin are less sharp (have smaller H) than the CTME discussed here, which will tend to rather large H.

Dickinson et al. [10] pointed out that a current–time curve at such an electrode should, at short times, behave in a Cottrellian manner, and demonstrate this by using a log–log plot, which has the required slope of −0.5 at small T for some H. Not only should this be the case, but also, if the current is normalised by the electrode area, the resulting current densities J for all H should collapse to the same curve at small H, as is the case for electrodes of all shapes [33]. This is observed in Fig. 4. The small differences between the curves at small T can be attributed to only a few time steps having been taken in the simulation, and there is always a larger error in these initial steps, which then becomes smaller as the simulation converges. But the effect appears to be reasonably demonstrated, and the slope is the same as that of a true Cottrellian curve, as is also shown in Fig. 4. This was effectively the current at a "shrouded disk" [34] of unity radius and normalised by its area, π. It lies slightly below the CTME curves, because there is better diffusional access

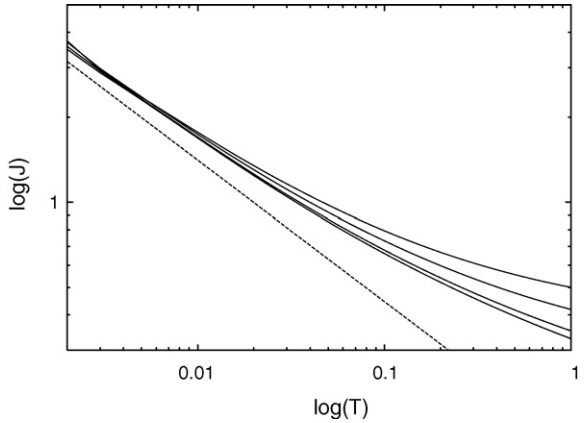

Fig. 4. Current density curves. Top to bottom: $H = 30, 10, 3, 1$. The dashed curve is the Cottrellian response at a shrouded disk.

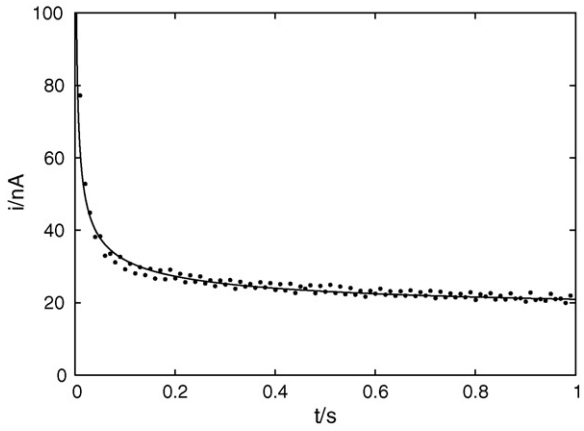

Fig. 5. Simulated current and experimental values. Fitted values were $a = 9.5$ μm, $h = 190$ μm (i.e. $H = 20$).

to the CTME than to a flat disk. The near-Cottrellian behaviour of the electrodes at short times can be used to estimate electrode area, from which the dimensions may be obtained, if the angle α is known (for example, from a scanning electron micrograph). The curves show that Cottrellian behaviour is seen at around $T \leq 0.01$, which can be translated into actual times using (4a).

Finally, a comparison between the experimental curve with a simulated one is presented in Fig. 5. The experimental curve was obtained by sampling the current at 4000 Hz. The fit was obtained by setting the base radius of the cone to 9.5 μm and h to 190 μm (i.e. $H = 20$) and setting the diffusion coefficient of $Ru(NH_3)_6^{3+}$ to the known value 7.7×10^{-10} m^2 s^{-1} [35]. For the experimental curve, only every 30th point is shown. The agreement between simulated and experimental points is reasonable. Therefore, fitting of the simulated chronoamperogram to an experimental chronoamperogram may aid in estimating the radius and the axial length of the cone of a freshly constructed CTME.

6. Conclusions

We have shown how to simulate chronoamperometic currents at a CTME to obtain results for varying H. For H close to zero, simulated currents converge to those at a disk electrode. For larger H, currents are larger, and for H greater than approximately 20, they approach those at a cylinder of length H and half the radius of the CTME. At short times, all currents are close to Cottrellian, which can be used to estimate electrode area and its dimensions. A reasonable simulation fit was obtained for an experimental

curve and can be used to determine electrode dimensions, if the diffusion coefficient and concentration of the electroactive substance are known. The CTME is rather easily prepared and may prove useful for electroanalysis in biological matrices. Further work is being conducted to produce smaller electrodes of nanometre scales.

Acknowledgements

JS acknowledges the European Commission, Marie Curie Transfer of Knowledge Programme (grant MTKD-CT-2005-029568) for funding. DB thanks Macquarie University for supporting his visit to the University.

References

[1] A. Hermans, R.B. Keithley, J.M. Kita, L.A. Sombers, R.M. Wightman, Anal. Chem. 80 (2008) 4040.
[2] L.A. Woods, P.R. Powell, T.L. Paxon, A.G. Ewing, Electroanalysis 17 (2005) 1192.
[3] M.A. Johnson, M. Villanueva, C.L. Haynes, A.T. Seipel, L.A. Buhler, R.M. Wightman, J. Neurochem. 103 (2007) 2102.
[4] M.A. Makos, Y. Kim, K. Han, M.L. Heien, A.G. Ewing, Anal. Chem. 81 (2009) 1848.
[5] K.J. Leck, C.D. Blaha, K.I. Matthaei, G.L. Forster, J. Holgate, I.A. Hendry, Neuropharmacology 51 (2006) 597.
[6] M. McNally, D.K.Y. Wong, Anal. Chem. 73 (2001) 4793.
[7] D.K.Y. Wong, C.D. Blaha, M. McNally, Chem. Aust. 70 (2003) 12.
[8] S. Alwarappan, K.S.A. Butcher, D.K. Wong, Sens. Actuators B 128 (2007) 299.
[9] C.G. Zoski, M.V. Mirkin, Anal. Chem. 74 (2002) 1986.
[10] E.J.F. Dickinson, I. Streeter, R.G. Compton, J. Phys. Chem. B 112 (2008) 4059.
[11] D. Britz, Digital Simulation in Electrochemistry, 3rd ed., Springer, Berlin, 2005.
[12] A. Szabo, D.K. Cope, D.E. Tallman, P.M. Kovach, R.M. Wightman, J. Electroanal. Chem. 217 (1987) 417.
[13] P.J. Mahon, K.B. Oldham, Electrochim. Acta 49 (2004) 5041.
[14] D. Britz, O. Østerby, J. Strutwolf, J. Electroanal. Chem. 622 (2008) 51.
[15] Y. Saito, Rev. Polarog. (Jpn.) 15 (1968) 177.
[16] D.J. Gavaghan, J. Electroanal. Chem. 456 (1998) 1.
[17] D. Britz, J. Strutwolf, Electrochim. Acta 52 (2006) 33.
[18] R. Seeber, S. Stefani, Anal. Chem. 53 (1981) 1011.
[19] S.W. Feldberg, J. Electroanal. Chem. 127 (1981) 1.
[20] J. Strutwolf, D. Britz, J. Electroanal. Chem. 566 (2004) 15.
[21] J. Crank, R.M. Furzeland, J. Inst. Maths. Appl. 20 (1977) 355.
[22] B. Fornberg, Math. Comp. 51 (1988) 699.
[23] W.G. Bickley, Math. Gaz. 25 (1941) 19.
[24] C.F. Curtiss, J.O. Hirschfelder, Proc. Natl. Acad. Sci. U.S.A. 38 (1952) 235.
[25] J. Mocak, S.W. Feldberg, J. Electroanal. Chem. 378 (1994) 31.
[26] D. Britz, J. Strutwolf, L. Thøgersen, J. Electroanal. Chem. 512 (2001) 119.
[27] P. Laasonen, Acta Math. 81 (1949) 309.
[28] I.S. Duff, J.K. Reid, ACM Trans. Math. Soft. 5 (1979) 18.
[29] http://hsl.rl.ac/archive/hslarchive.html.
[30] W.H. Press, S.A. Teukolsky, W.T. Vetterling, B.P. Flannery, Numerical Recipes in Fortran, 2nd ed., Cambridge University Press, Cambridge, 1986.
[31] T.A. Davies, ACM Trans. Math. Software 30 (2004) 196.
[32] http://www.gnuplot.info.
[33] J.C. Myland, K.B. Oldham, J. Electroanal. Chem. 288 (1990) 1.
[34] K.B. Oldham, J. Electroanal. Chem. 122 (1981) 1.
[35] T.L. Ferreira, T.R.L.C. Paixão, E.M. Richter, O.A. El Seoud, M. Bertotti, J. Phys. Chem. B 111 (2007) 12478.